

# A Modified Maximum Entropy Algorithm for Sea-Land Segmentation

Shaheera Rashwan<sup>1\*</sup>, Hesham M. Helal<sup>2</sup>

Submitted: 10/09/2022 Accepted: 20/12/2022

**Abstract:** Sea-land segmentation is a key pre-processing step for ship detection from optical remote sensing imagery. Because of waves, illumination and shadows, conventional sea-land segmentation algorithms usually confuse between land and sea. Thus, a new maximum entropy segmentation scheme based on an adaptive threshold is proposed in this paper. Experimental results show that our algorithm has better accuracy compared to many traditional algorithms such as conventional maximum entropy algorithm, Otsu algorithm and bimodal histogram algorithm.

**Keywords:** Maximum entropy, Remote sensing, Sea land segmentation, Ship detection

## 1. Introduction

Automatic coastline extraction from satellites is a fundamental task to map coastal regions and to detect ships and small vessels, and sea-land segmentation is the main technology of coastline extraction. The development of satellite remote sensing technology had provided tons of high-resolution images of the coastal area that can be used for sea land segmentation [1].

The sea land segmentation methods mainly include threshold segmentation methods, edge-based methods, active contour method, and machine learning methods methods.

The threshold segmentation methods are methods that set a threshold value according to the image gray level to segment the land and sea. Guo et al. [2] proposed a method that used a normalized difference water index (NDWI) to segment sea and land. Chen et al. [3] used the tasseled cap transformation to extract sea-land information. Wernette et al. [4] presented a multi-scale relief method to extract the morphology of the barrier island from high-resolution digital elevation models (DEM). A key of these methods is the good choice of the threshold.

The edge-based methods apply the distinguished edge feature to segment the images. Wang and Liu [5] proposed a ridge-tracing method using the statistics of the pixel intensities in the land region and sea region to determine the boundary. These methods

are fine for the detection of clear boundaries but they are deeply affected by noise.

The active contour methods are segmentation methods that use energy forces and constraints to separate the region of interest from an image. Cao et al. [6] proposed a new geometric active contour model adaptive to the speckle noises for sea land segmentation from SAR images. Fan et al. [7] proposed a level set approach with a particle swarm optimization algorithm. Elkhateeb et al. [8] proposed a modified Chan–Vese method for sea–land segmentation with fuzzy c-means.

Machine learning methods apply useful information and prior knowledge based on a variety of data to segment the sea-land regions. Rigos et al. [9] and Vos et al. [10] used a neural network to extract the shoreline from satellite images. Sun et al. [11] adopted a superpixel-based conditional random field model to detect the sea and land areas. Cheng et al. [12] proposed a graph cut method with a probabilistic support vector machine to segment the sea and land regions.

Some convolutional neural network (CNN) methods were introduced recently in coastline extraction by segmenting the land and sea. Liu et al. [13] used a CNN with leaky rectified linear unit (leaky-ReLU) activation function. Liu W et al. [14] adopted a multitask CNN without downsampling to get shorelines from remote sensing images. Cui et al. [15] proposed a scale-adaptive CNN for sea–land segmentation. Although the CNNs achieve good performances, buying the remote sensing images directly from their providers is too expensive and obtaining many satellites map images freely from the web map services is difficult. Also, the ground truth of these data cannot be easily determined to train the network for the sea-land region extraction.

The rest of the study has the following sections. Methodology suggests details about the new method used and its background. Results reports details about the dataset, the quality metrics used for evaluation and also the experimental results with a

<sup>1</sup> Informatics Research Institute, City of Scientific Research and Technological Applications, Alexandria, Egypt. ORCID ID : 0000-0003-3536-5109

<sup>2</sup> Maritime Postgraduate Studies Institute, Arab Academy for Science, Technology & Maritime Transport (AASTMT), Alexandria, Egypt

ORCID ID : 0000-3343-7165-777X

<sup>3</sup> Computer Eng., Selcuk University, Konya – 42002, TURKEY  
ORCID ID : 0000-3343-7165-777X

\* Corresponding Author Email: author@email.com

discussion. The last section concludes and discusses future directions in research in this area.

## 2. Methodology

### 2.1 Maximum Entropy Algorithm

Constantino Tsallis presented in 1988 a new definition of the entropic function in order to be used in a non-extensive thermodynamics [16]. The first paper that applied Tsallis entropy on image thresholding was in 2004 [17].

The images are composition of pixels that have discrete gray level values. So, a discrete set of probabilities  $\{p_i\}$ , with random variable  $i$  is presented here. Condition on probabilities is:  $\sum_i p_i = 1$ .

Tsallis entropy is defined as:

$$S_q = \frac{k}{q-1} (1 - \sum_i p_i^q) \quad (1)$$

Where  $q$  is real parameter and  $k$  is constant equals 1 for image processing

For a bi-level threshold  $t$  of the gray levels, the Tsallis entropies are defined as [17]:

$$S_q^A(t) = \frac{1}{q-1} \left\{ 1 - \sum_{i=1}^t \left( \frac{p_i}{p_A} \right)^q \right\}; S_q^B(t) = \frac{1}{q-1} \left\{ 1 - \sum_{i=t+1}^k \left( \frac{p_i}{p_B} \right)^q \right\} \quad (2)$$

Where A and B are two independent systems (e.g. Sea and Land areas)

The total entropy is:

$$S_q(t) = S_q^A(t) + S_q^B(t) + (1-q)S_q^A(t)S_q^B(t) \quad (3)$$

When this entropy is maximized, the corresponding gray level  $t$  is considered the optimum threshold value [17]. One drawback to this approach is the need to select a good threshold  $t$  in order to get high segmentation accuracy.

### 2.2 Modified Maximum Entropy Algorithm

It is clear from section 2.1 that the bi-level thresholding segmentation highly depends on the choice of the threshold  $t$ . Hence, we develop our new algorithm for sea-land segmentation by estimating a good threshold. The new threshold is based on statistics considering the sea region.

The new algorithm is as follows

#### Algorithm 1: Modified Maximum Entropy

*Inputs:* Satellite Image  $I$ , Initial threshold  $t$

*Output:* Segmented Image  $O$

**Step 1:** Apply the Tsallis threshold segmentation using  $t$  to get sea region and land region of the input image  $I$

**Step 2:** Calculate mean  $\mu$  for the sea region by adding all pixel values in the sea region then divide by their number

**Step 3:** Calculate new threshold. The threshold for sea-land segmentation is as follows:  $T = \lambda \mu$  Where  $\lambda$  is the weight of mean ( $\mu$ ).

**Step 4:** Run the maximum entropy algorithm for sea land segmentation with the new threshold  $T$  to get the final segmented image  $O$

Here, we choose  $\lambda = 1.3$  for considering the gaussian distribution of the pixel values in the image and also for the illumination on the sea surface

## 3. Experimental Results

### 3.1 Materials and Dataset

Eight Landsat-8 OLI remote sensing images were used as experimental data. These images were extracted from a sea-land benchmark dataset using Landsat-8 Operational Land Imager (OLI) imagery consisting of 18,000 km<sup>2</sup> of coastline around China [18-19]

The semantic annotation of this dataset was done [18] by dividing pixels of all images into two classes: sea and land. Ground truth images were first labelled for all images with LabelMe [20] taking into account the properties of different coastlines then the land positions and the coastlines standards were extracted using OpenStreetMap [21] data. Finally, disturbing images with cloud and large blank areas were removed from the dataset.

### 3.2 Quality Metrics

In the experiments, *Precision*, *Recall*, *F1 score*, and the accuracy of sea and land areas are used as quality metrics to evaluate the results of different segmentation methods, their formulas [22] are defined as:

$$Precision = \frac{TP}{TP+FP} \quad (4)$$

$$Recall = \frac{TP}{TP+FN} \quad (5)$$

$$F1 \text{ score} = \frac{2 * Precision * Recall}{Precision + Recall} \quad (6)$$

$$Accuracy = \frac{TP+TN}{TP+TN+FP+FN} \quad (7)$$

where TP is the number of pixels of land classified as land, FP is the number of pixels of sea classified as land, TN is the number of pixels of sea classified as sea, and FN is the number of pixels of land classified as sea.

Precision denotes the number of positive class predictions that actually belong to the positive class while Recall (Sensitivity) denotes the number of positive class predictions taken from all positive samples in the dataset.

F1 score represents the score that balances the precision and recall in one term

The accuracy is the ratio of the number of samples correctly classified to the total number of samples of the dataset.

### 3.3 Results and Discussion

In these experiments, we set Lambda =1.3 and Threshold of Maximum Entropy= 0.8. All implementations in this paper were performed using Python 3.7.

In this subsection, Figures (1-8) and Tables (1-8) show the subjective and the objective evaluations, respectively, of the new algorithm compared to the Otsu algorithm [23], the bimodal histogram algorithm [24] and the conventional maximum entropy algorithm [17].

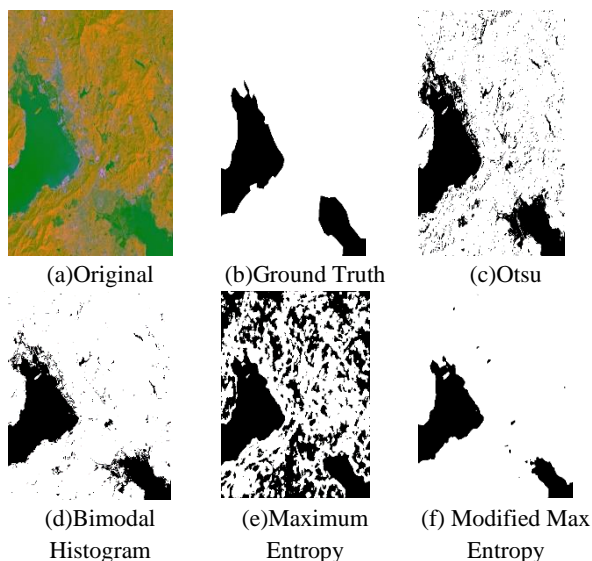


Figure 1. The first image sample

Table 1. Quality Metrics for the different algorithms applied on the first image sample

	Otsu	Bimodal Hist.	MaxEntropy	Modified MaxEntropy
<b>Precision</b>	0.6591	0.8201	0.3286	<b>0.9850</b>
<b>Recall</b>	<b>0.9732</b>	0.9390	0.9419	0.8316
<b>F1 score</b>	0.7859	0.8755	0.4872	<b>0.9018</b>
<b>Accuracy</b>	0.9143	0.9568	0.6796	<b>0.9707</b>

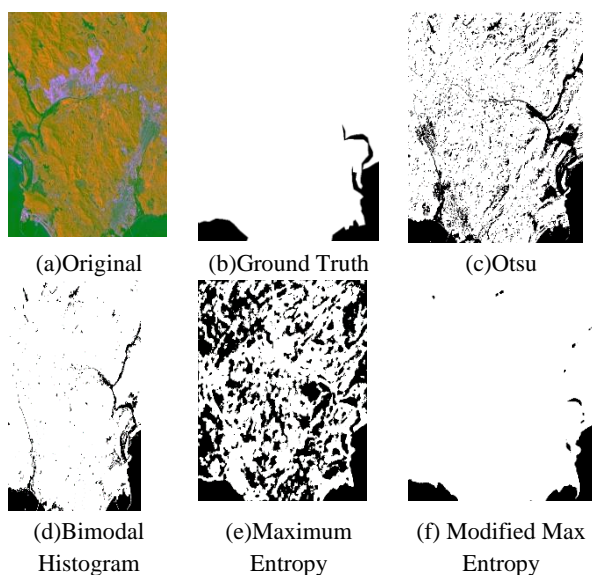


Figure 2. The second image sample

Table 2. Quality Metrics for the different algorithms applied on the second image sample

	Otsu	Bimodal Hist.	MaxEntropy	Modified MaxEntropy
<b>Precision</b>	0.3498	0.6678	0.1606	<b>0.9728</b>
<b>Recall</b>	<b>0.9781</b>	0.9387	0.9479	0.7939
<b>F1 score</b>	0.5154	0.7804	0.2747	<b>0.8743</b>
<b>Accuracy</b>	0.8737	0.9637	0.6562	<b>0.9843</b>

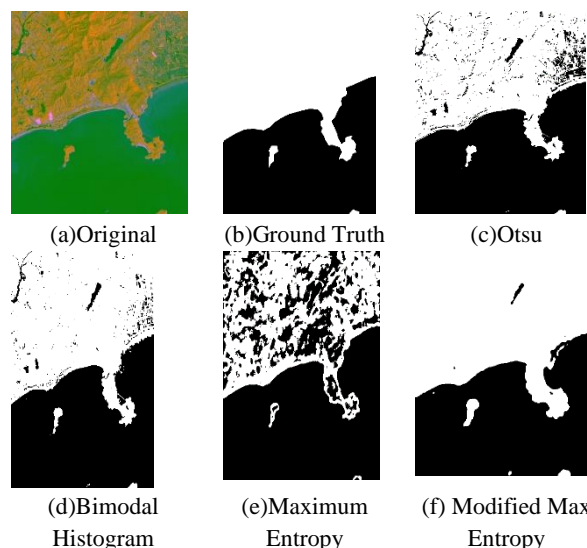
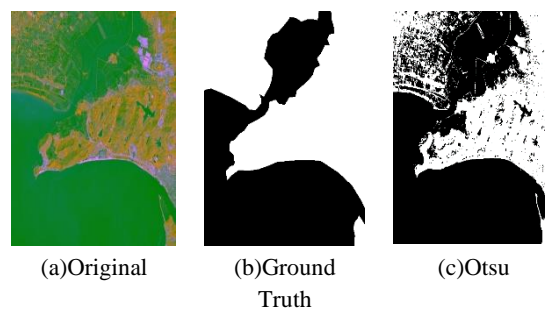
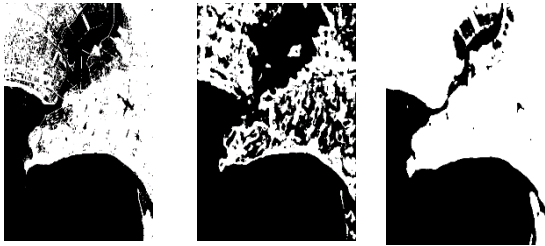


Figure 3. The third image sample

Table 3. Quality Metrics for the different algorithms applied on the third image sample

	Otsu	Bimodal Hist.	MaxEntropy	Modified Max Entropy
<b>Precision</b>	0.9126	0.9546	0.7243	<b>0.9959</b>
<b>Recall</b>	0.9840	0.9766	<b>0.9889</b>	0.9396
<b>F1 score</b>	0.9470	0.9654	0.8361	<b>0.9669</b>
<b>Accuracy</b>	0.9479	0.9669	0.8167	<b>0.9696</b>





(d)Bimodal Histogram (e)Maximum Entropy (f) Modified Max Entropy

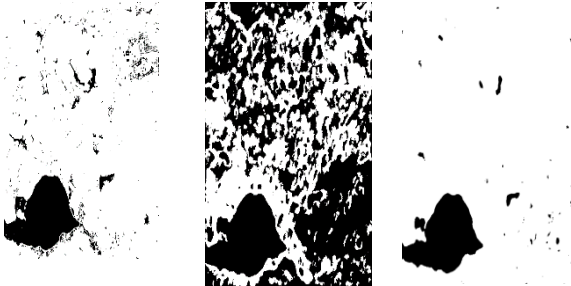
Figure 4. The fourth image sample

Table 4. Quality Metrics for the different algorithms applied on the fourth image sample

	Otsu	Bimodal Hist.	MaxEntropy	Modified Max Entropy
<b>Precision</b>	0.7762	0.8608	0.6947	<b>0.9962</b>
<b>Recall</b>	0.9795	0.9612	<b>0.9802</b>	0.8370
<b>F1 score</b>	0.8661	0.9082	0.8131	<b>0.9097</b>
<b>Accuracy</b>	0.8494	0.9034	0.7760	<b>0.9174</b>



(a)Original (b)Ground Truth (c)Otsu



(d)Bimodal Histogram (e)Maximum Entropy (f) Modified Max Entropy

Figure 5. The fifth image sample

Table 5. Quality Metrics for the different algorithms applied on the fifth image sample

	Otsu	Bimodal Hist.	MaxEntropy	Modified Max Entropy
<b>Precision</b>	0.4428	0.7039	0.1545	<b>0.9218</b>
<b>Recall</b>	<b>0.9637</b>	0.9360	0.9546	0.8743
<b>F1 score</b>	0.6068	0.8036	0.2659	<b>0.8974</b>
<b>Accuracy</b>	0.8895	0.9595	0.5337	<b>0.9823</b>



(a)Original (b)Ground Truth (c)Otsu

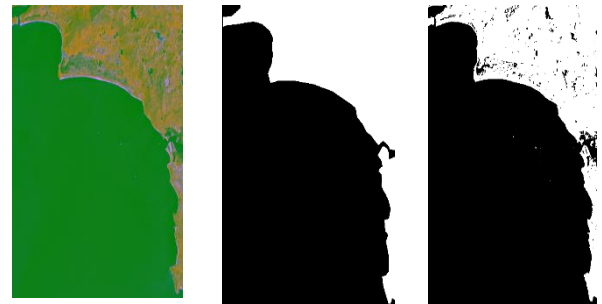


(d)Bimodal Histogram (e)Maximum Entropy (f) Modified Max Entropy

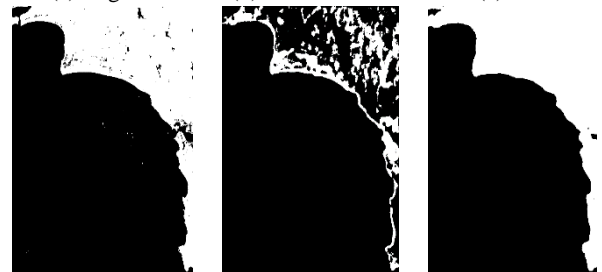
Figure 6. The sixth image sample

Table 6. Quality Metrics for the different algorithms applied on the sixth image sample

	Otsu	Bimodal Hist.	MaxEntropy	Modified Max Entropy
<b>Precision</b>	0.8165	0.8249	0.6751	<b>0.9699</b>
<b>Recall</b>	<b>0.9958</b>	0.9952	0.9943	0.9649
<b>F1 score</b>	0.8973	0.9021	0.8042	<b>0.9674</b>
<b>Accuracy</b>	0.8713	0.8780	0.7266	<b>0.9633</b>



(a)Original (b)Ground Truth (c)Otsu



(d)Bimodal Histogram (e)Maximum Entropy (f) Modified Max Entropy

Figure 7. The seventh image sample

**Table 7.** Quality Metrics for the different algorithms applied on the seventh image sample

	Otsu	Bimodal Hist.	MaxEntropy	Modified Max Entropy
<b>Precision</b>	0.9768	0.9870	0.8065	<b>0.9999</b>
<b>Recall</b>	<b>0.9963</b>	0.9953	<b>0.9963</b>	0.9753
<b>F1 score</b>	0.9865	<b>0.9911</b>	0.8914	0.9875
<b>Accuracy</b>	0.9802	<b>0.9871</b>	0.8240	0.9821

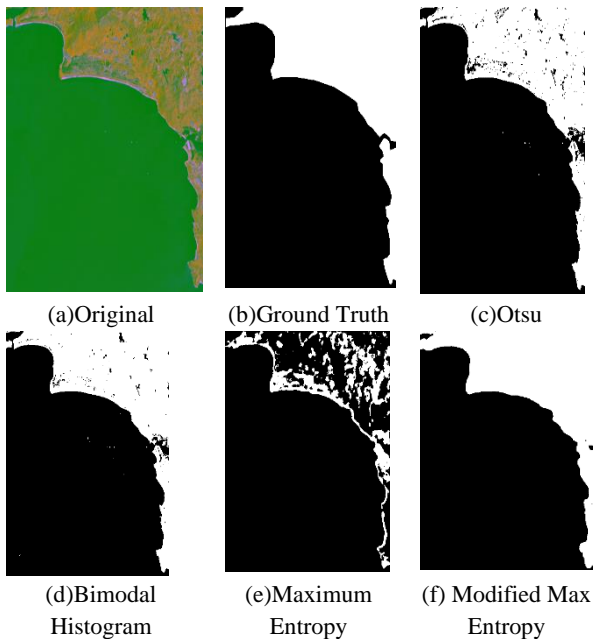


**Figure 8.** The eighth image sample

**Table 8.** Quality Metrics for the different algorithms applied on the eighth image sample

	Otsu	Bimodal Hist.	MaxEntropy	Modified Max Entropy
<b>Precision</b>	0.8448	0.9019	0.3556	<b>0.9274</b>
<b>Recall</b>	<b>0.9888</b>	0.9845	0.9820	0.9477
<b>F1 score</b>	0.9111	<b>0.9413</b>	0.5221	0.9375
<b>Accuracy</b>	0.9467	<b>0.9661</b>	0.5036	0.9651

**Table 9.** Average Quality Metrics for the different algorithms over the eight images

	Otsu	Bimodal Hist.	MaxEntropy	Modified Max Entropy
<b>Precision</b>	0.7223	0.8401	0.4875	<b>0.9711</b>
<b>Recall</b>	<b>0.9824</b>	0.9658	0.9733	0.8955
<b>F1 score</b>	0.8145	0.8960	0.6119	<b>0.9303</b>
<b>Accuracy</b>	0.9091	0.9477	0.6895	<b>0.9669</b>

From the objective evaluation presented in Tables (1-6), we can see that the new modified Maximum Entropy Algorithm outperforms the state-of-the-art algorithms used for comparison in terms of three quality metrics: the Precision, the F1-score and the Accuracy.

However, in Tables (7-8), the bimodal histogram is the best in terms of F1-score and Accuracy with slight differences between it and our algorithm in those two images while the new algorithm outperforms the other algorithms used in comparison in terms of Precision in the eight images.

The metric recall changes the best algorithm from an image to another although the subjective evaluation using images from Figures (1-8) where it is clear by the eye observation that this metric does not describe which is the best algorithm in most cases. The reason for this can be explained by: "Precision is a measure of quality, and recall is a measure of quantity". High recall values mean that an algorithm returns most of the relevant results not necessary to return also irrelevant ones and hence recall is not always a significant metric to evaluate the segmentation

According to Table 9 where we calculate the average over the eight images, our algorithm has the best values in Precision (0.9711), F1-score (0.9303) and Accuracy (0.9669)

#### 4. Conclusions and Future Work

The sea land segmentation constitutes a necessary step in the process of ship detection from optical satellite images. In this paper, we presented a novel approach to segment sea-land areas using an adaptive threshold to the Tsallis maximum entropy bi-level thresholded segmentation algorithm. Our threshold depended on the statistical properties of the pixels' intensities in the sea region. The new method showed high efficiency comparing to three of the state-of-the-art sea land segmentation methods when it was applied to eight different Landsat-8 OLI satellite images of a public dataset.

As future research directions, we suggest the determination of the range of  $\lambda$  based on the illumination of the sea region in the satellite images.

#### Funding Statement:

No funding was received for this study.

#### Data Availability Statement:

Data used in this study is publicly available.

#### Competing Interest statement:

The authors declare they have no competing interests.

#### Author Contributions statement:

All authors contributed to the study conception and design. Material preparation, data collection and analysis were performed by Rashwan. The first draft of the manuscript was written by Rashwan and revised by Helal. All authors read and approved the final manuscript.

#### References

- [1]. Roelfsema, C., Kovacs, E. M., Saunders, M. I., Phinn, S., Lyons, M., and Maxwell, P. (2013). Challenges of Remote

- Sensing for Quantifying Changes in Large Complex Seagrass Environments. *Estuarine Coastal Shelf Sci.* 133, 161–171.
- [2]. Chaudhary, D. S. . (2022). Analysis of Concept of Big Data Process, Strategies, Adoption and Implementation. *International Journal on Future Revolution in Computer Science & Communication Engineering*, 8(1), 05–08. <https://doi.org/10.17762/ijfrcsce.v8i1.2065>
  - [3]. Guo, Q., Pu, R., Zhang, B., and Gao, L. (2016). “A Comparative Study of Coastline Changes at Tampa Bay and Xiangshan Harbor During the Last 30 Years,” in 2016 IEEE International Geoscience and Remote Sensing Symposium, Beijing, China, July 10–15, 2016 (IGARSS), 5185–5188.
  - [4]. André Sanches Fonseca Sobrinho. (2020). An Embedded Systems Remote Course. *Journal of Online Engineering Education*, 11(2), 01–07. Retrieved from <http://onlineengineeringeducation.com/index.php/joe/article/view/39>
  - [5]. Chen, C., Fu, J., Zhang, S., and Zhao, X. (2019). Coastline Information Extraction Based on the Tasseled Cap Transformation of Landsat-8 OLI Images. *Estuarine Coastal Shelf Sci.* 217, 281–291.
  - [6]. Wernette, P., Houser, C., and Bishop, M. P. (2016). An Automated Approach for Extracting Barrier Island Morphology from Digital Elevation Models. *Geomorphology* 262, 1–7.
  - [7]. Wang, D., and Liu, X. (2019). Coastline Extraction from SAR Images Using Robust Ridge Tracing. *Mar. Geodesy* 42, 286–315.
  - [8]. Cao, K., Fan, J., Xinxin Wang, X., Xiang Wang, X., Jianhua Zhao, J., and Fengshou Zhang, F. (2016). “Coastline Automatic Detection Based on High Resolution SAR Images,” in 2016 4th International Workshop on Earth Observation and Remote Sensing Applications, Guangzhou, China, July 4–6, 2016 (EORSA), 43–46.
  - [9]. Sai, M. P. ., V. A. . Rao, K. . Vani, and P. . Poul. “Prediction of Housing Price and Forest Cover Using Mosaics With Uncertain Satellite Imagery”. *International Journal on Recent and Innovation Trends in Computing and Communication*, vol. 10, no. 8, Aug. 2022, pp. 36-46, doi:10.17762/ijritcc.v10i8.5666.
  - [10]. Fan, J., Cao, K., Zhao, J., Jiang, D., and Tang, X. (2016). “A Hybrid Particle Swarm Optimization Algorithm for Coastline SAR Image Automatic Detection,” in 2016 12th World Congress on Intelligent Control and Automation, Guilin, China, June 12–15, 2016 (WCICA), 822–825.
  - [11]. Elkhateeb, E., Soliman, H., Atwan, A., Elmogy, M., Kwak, K.-S., and Mekky, N. (2021). A Novel Coarse-To-Fine Sea-Land Segmentation Technique Based on Superpixel Fuzzy C-Means Clustering and Modified Chan-Vese Model. *IEEE Access* 9, 53902–53919
  - [12]. Rigos, A., Tsekouras, G. E., Vousdoukas, M. I., Chatzipavlis, A., and Velegarakis, A. F. (2016). A Chebyshev Polynomial Radial Basis Function Neural Network for Automated Shoreline Extraction from Coastal Imagery. *ICA* 23, 141–160.
  - [13]. Vos, K., Splinter, K. D., Harley, M. D., Simmons, J. A., and Turner, I. L. (2019). CoastSat: A Google Earth Engine-Enabled Python Toolkit to Extract Shorelines from Publicly Available Satellite Imagery. *Environ. Model. Softw.* 122, 104528.
  - [14]. Sun, B., Li, S., and Xie, J. (2019). “Sea-Land Segmentation for Harbour Images with Superpixel CRF,” in IGARSS 2019 - 2019 IEEE International Geoscience and Remote Sensing Symposium, Yokohama, Japan, July 28–August 2, 2019, 3899–3902.
  - [15]. Cheng, D., Meng, G., Xiang, S., and Pan, C. (2016). Efficient Sea-Land Segmentation Using Seeds Learning and Edge Directed Graph Cut. *Neurocomputing* 207, 36–47.
  - [16]. Liu, X.-Y., Jia, R.-S., Liu, Q.-M., Zhao, C.-Y., and Sun, H.-M. (2019). Coastline Extraction Method Based on Convolutional Neural Networks-A Case Study of Jiaozhou Bay in Qingdao, China. *IEEE Access* 7, 180281–180291.
  - [17]. Liu W, W., Chen, X., Ran, J., Liu, L., Wang, Q., Xin, L., et al. (2021). LaeNet: A Novel Lightweight Multitask CNN for Automatically Extracting Lake Area and Shoreline from Remote Sensing Images. *Remote Sensing* 13, 56.
  - [18]. Cui, B., Jing, W., Huang, L., Li, Z., and Lu, Y. (2021). SANet: A Sea-Land Segmentation Network via Adaptive Multiscale Feature Learning. *IEEE J. Sel. Top. Appl. Earth Obs. Remote Sensing* 14, 116–126.
  - [19]. Tsallis, C. (1988). Possible generalization of Boltzmann-Gibbs statistics. *Journal of Statistical Physics*, 52, 479–487.
  - [20]. Portes de Albuquerque, M.; Esquef, I.A.; Gesualdi Mello, A.R.; Portes de Albuquerque, M. (2004). Image thresholding using Tsallis entropy. *Pattern Recognition Letters*, 25, 1059-1065.
  - [21]. Yang T, Jiange S, Hong Z, Zhang Y, Han Y, Zhou R, Wang J, Yang S, Tong X, Kuc TY. Sea-Land Segmentation Using Deep Learning Techniques for Landsat-8 OLI Imagery. *Marine geodesy*, 2020,43(2):105-133.
  - [22]. Sea Land Segmentation Public Dataset (<https://github.com/zhongsh/sea-land-segmentation>) Last accessed: 16 April 2022
  - [23]. Russell, B. C., A. Torralba, K. P. Murphy, and W. T. Freeman. 2008. LabelMe: a database and web-based tool for image annotation. *International Journal of Computer Vision* 77(1-3): 157-173.
  - [24]. Modiya, P., & Vahora, S. (2022). Brain Tumor Detection Using Transfer Learning with Dimensionality Reduction Method. *International Journal of Intelligent Systems and Applications in Engineering*, 10(2), 201–206. Retrieved from <https://ijisae.org/index.php/IJISAE/article/view/1310>
  - [25]. Haklay, M. and P. Weber. 2008. OpenStreetMap: User-generated street maps. *IEEE Pervasive Computing* 7(4): 12-18.
  - [26]. Sokolova, M., N. Japkowicz, and S. Szpakowicz. 2006. Beyond accuracy, F-score and ROC: a family of discriminant measures for performance evaluation. In *Proceedings of the Australasian Joint Conference on Artificial Intelligence* Springer, Berlin, Heidelberg: 1015-1021.
  - [27]. Nobuyuki Otsu (1979). "A threshold selection method from gray-level histograms". *IEEE Trans. Sys. Man. Cyber.* 9 (1): 62–66.
  - [28]. Chow, C.K. and Kaneko, T., 1972. Automatic boundary detection of the left ventricle from cineangiograms. *Computers and biomedical research*, 5(4), pp.388-410.